

Improvement of visible light responsivity of rutile TiO₂ nanorods by site-selective modification of iron(III) ion on newly exposed faces formed by chemical etching treatment

Misa Nakamura^a, Asami Ono^a, Eunyoung Bae^a, Naoya Murakami^a, Teruhisa Ohno^{a,b,c,*}

^a Department of Materials Science, Faculty of Engineering, Kyushu Institute of Technology, 1-1 Sensuicho, Tobata, Kitakyushu 804-8550, Japan

^b JST, PRESTO, 4-1-8 Honcho Kawaguchi, Saitama 332-0012, Japan

^c JST, ACT-C, 4-1-8 Honcho Kawaguchi, Saitama 332-0012, Japan

abstract

cation of trivalent iron(III) (Fe³⁺) ions was applied to rutile titanium(IV) oxide (TiO₂) nanorods after chemical etching treatment in order to improve photocatalytic visible-light irradiation. Chemical etching of rutile nanorods with {1 1 0} and {1 1 1} faces using aqueous sulfuric acid (H₂SO₄) or hydrogen peroxide (H₂O₂)–ammonia (NH₃) solution, respectively. Fe³⁺-modified rutile nanorods after chemical etching exhibited higher photocatalytic activity for degradation of toluene than before chemical etching. This improvement of photocatalytic activity was attributed to a large amount of site-selectively-modified Fe³⁺ ions, resulting in an increase in adsorption. Moreover, our results indicate that a rutile nanorod with large {0 0 1} and {1 1 0} exposed crystal faces is the most suitable structure for visible light effective modification of Fe³⁺ ions.

1. Introduction

Titanium(IV) oxide (TiO₂) has been a useful photocatalyst in terms of its oxidation ability, stability and availability. It shows high photocatalytic activities for decomposition of organic pollutants under ultraviolet (UV) light irradiation. TiO₂ photocatalysts have been developed for many applications, and their efficiency under visible-light irradiation has been improved by doping of transition metal ion [1–3], nitrogen [4,5], sulfur [6,7], and carbon [8,9]. Recently, some visible-light-responsive TiO₂ photocatalysts have been developed by modification with a metal surface complex that works as a sensitizer for visible light [10–13]. This method has the advantages of simple preparation and no introduction of defects in TiO₂. We have reported that modification of trivalent iron(III) (Fe³⁺) ions on rutile TiO₂ greatly improved activity for acetaldehyde decomposition under visible-light irradiation [14]. That study indicated that photoexcited Fe³⁺ ions injected electrons into the conduction band of TiO₂ as a counterpart of oxidation by the oxidized state of Fe³⁺ ions under visible-light irradiation. Thus, Fe³⁺ ions work as visible light sensitizers and oxidation sites. Hence, modification with an excess amount of Fe³⁺ ions might decrease photocatalytic activity due to inefficient reduction, resulting in

back electron transfer from TiO₂ into the oxidized state of Fe³⁺ ions. Therefore, it is important to ensure moderate reduction sites and visible-light absorption.

In our previous study, Fe³⁺ ions were selectively modified on specific sites of rutile TiO₂ [15]. This modification employs characteristic adsorption properties of Fe³⁺/Fe²⁺ ions on TiO₂ and redox reaction over rutile TiO₂ nanorods with {1 1 0} and {1 1 1} exposed crystal faces. It has been reported that Fe²⁺ ions are desorbed on TiO₂, whereas Fe³⁺ ions are easily adsorbed on TiO₂ [14]. Therefore, it is thought that modification of Fe³⁺ ions on TiO₂ under UV irradiation induces site-selective modification of Fe³⁺ ions on oxidation sites of TiO₂. Moreover, utilization of rutile TiO₂ particles with exposed crystal faces is expected to improve site selectivity of Fe³⁺-modification because separation of redox reaction occurs on the rutile nanorods [15]. As a result, Fe³⁺ ions were modified mainly on {1 1 1} faces as oxidation faces of the rutile nanorods, and this sample showed high activity for acetaldehyde decomposition under visible-light irradiation because of spatial separation of redox sites.

However, the rutile nanorods have large {1 1 0} faces as reduction sites and small {1 1 1} faces as oxidation sites, and the surface area of {1 1 1} faces is only 6% of the total surface area. Thus, it is difficult for further enhancement of photocatalytic activity using these rutile nanorods because the surface area of oxidation faces limits the amount of site-selective-modified Fe³⁺ ions, which absorb visible light. One possible solution is further control of the surface

morphology, especially oxidation faces. We have reported that new active crystal faces, i.e., $\{01\}$ and $\{1n\}$ ($n < 1$) faces, are easily exposed by chemical etching treatment of rutile nanorods with aqueous hydrogen (H_2O_2)–ammonia (NH_3) or sulfuric acid (H_2SO_4) solution [16]. Newly exposed crystal faces exhibited superior oxidation ability, resulting in enhancement of photocatalytic activity for toluene decomposition under UV irradiation. Therefore, newly exposed faces are expected to improve photocatalytic activity as a result of the different adsorption property of Fe^{3+} ions and/or formation of highly active Fe^{3+} ions on the faces.

In the present study, site-selective modification of Fe^{3+} ions was applied to rutile nanorods after morphological control by chemical etching treatment, and the relationship between newly exposed faces and photocatalytic activity under visible-light irradiation was examined. Also, electron transfer properties of Fe^{3+} -modified rutile nanorods were also analyzed by double-beam photoacoustic (DB-PA) spectroscopy.

2. Experimental

2.1. Sample preparation

2.1.1. Preparation of pure rutile TiO_2 nanorods [17,18]

The starting material for rutile TiO_2 nanorods was synthesized by hydrothermal treatment of aqueous titanium(III) chloride (0.15 mol dm^{-3}) solution containing sodium chloride (5 mol dm^{-3}) at 200°C for 6 h. The residue was centrifuged and rinsed with deionized water and then dried in a vacuum oven. This sample was denoted as nE sample.

2.1.2. Chemical etching with H_2SO_4 or H_2O_2 – NH_3 [16]

For chemical etching of rutile nanorods with H_2SO_4 , the synthesized nE sample (0.5 g) was added to concentrated H_2SO_4 (20 dm^3) in a flask. After stirring at room temperature for 15 h, nanorods were filtered and washed with 1% aqueous NH_3 solution and then with deionized water. The residue was dried at 70°C in air. This sample was denoted as ES sample.

For chemical etching of rutile nanorods with H_2O_2 – NH_3 , the synthesized nE sample (0.5 g) was added to 30% aqueous H_2O_2 (50 dm^3) and 2.5% aqueous NH_3 solution (5.0 dm^3) in a flask. After stirring at room temperature for 1 h, nanorods were separated by filtration, washed with water several times, and dried at 70°C in air. This sample was denoted as EH sample.

2.1.3. Site-selective modification of specific exposed faces with Fe^{3+} ions [15]

An aqueous suspension composed of prepared nanorods and an aqueous solution of iron(III) nitrate with ethanol was stirred for 6 h under an aerated condition. The stirring was carried out under UV irradiation with a 500 W super-high-pressure mercury lamp (Ushio, SX-UI501UO), the light intensity of which was 1.0 mW cm^{-2} . The supernatant and residue were separated by filtration immediately after stirring. The residue was washed with deionized water several times until the ionic conductivity of the supernatant was $<10 \text{ S cm}^{-1}$, and then the nanorods were dried in a vacuum oven.

2.2. Characterization

The crystal structures of the nanorods were confirmed by using an X-ray diffractometer (XRD; Rigaku, MiniFlex II) with $\text{Cu-K}\alpha$ radiation ($\lambda = 1.5405 \text{ \AA}$). The specific surface areas (S_{BET}) of nanorods were determined with a surface area analyzer (Quantachrome, Nova 4200e) using the Brunauer–Emmett–Teller equation. The morphology of the nanorods was observed by field emission scanning electron microscopy (FE-SEM; JEOL, JSM-6701FONO) and

transmission electron microscopy (TEM; Hitachi, H-9000NAR). The net amount of Fe^{3+} ions on the nanorod surface was estimated by analysis of the filtrate using inductively coupled plasma optical emission spectroscopy (ICP-OES; Shimadzu, ICPS-8000). The diffuse reflectance (DR) spectra were measured using a UV–vis spectrophotometer (Shimadzu, UV-2500PC) equipped with an integrating sphere unit (Shimadzu, ISR-240A).

2.3. Photocatalytic activity evaluation under visiblelight

The photocatalytic activities of the nanorods were evaluated by photocatalytic decomposition of toluene in gas phase. One hundred milligrams of powder, which has complete extinction of the incident radiation, was spread on a glass dish (5.6 cm^2), and the glass dish was placed in a 125 cm^3 Tedlar bag (AS ONE Co. Ltd.). One hundred parts per million of gaseous toluene was injected into the Tedlar bag, and photoirradiation was performed at room temperature after the toluene had reached an adsorption equilibrium. A light-emitting diode (LED; Lumileds, Luxeon LXHL-NRR8), which emitted light at a wavelength of ca. 455 nm with an intensity of 1.0 mW cm^{-2} , was used for visible-light irradiation. After the irradiation was started, the evolved carbon dioxide (CO_2) concentration was measured using a gas chromatograph (Shimadzu, GC-8A) equipped with a Porapak N packed column, flame ionization detector (FID) and a methanizer (GL Science, MT-221). Toluene was analyzed by a gas chromatograph (Shimadzu, GC-1700AF) equipped with an FID and a TC-1 capillary column.

2.4. DB-PA spectroscopic measurement

A gas-exchangeable photoacoustic (PA) cell equipped with two valves for gas flow was used, and a sample was placed in the cell. The atmosphere was controlled by a flow of artificial air or N_2 containing ethanol vapor (air + EtOH, N_2 + EtOH), and measurements were conducted after shutting off the valves, i.e., in a closed system at room temperature. An LED emitting light at ca. 625 nm (Lumileds, Luxeon LXHL-ND98) was used as a probe light, and the output intensity was modulated by a digital function generator (NF, DF1905) at 80 Hz. In addition to the modulated light, a blue-LED (Lumileds, Luxeon LXHL-NB98, emitting light at ca. 470 nm, 8.1 mW cm^{-2}) was also used as simultaneous continuous irradiation for photoexcitation. The PA signal acquired by a condenser microphone buried in the cell was amplified and monitored by a digital lock-in amplifier (NF, LI5640). Detailed setups of DB-PA spectroscopic measurements have been reported previously [19].

3. Results and discussion

3.1. Physical and chemical properties of the hydrothermally prepared rutile TiO_2 nanorods

The crystal structure of the hydrothermally prepared nE sample was attributed to pure rutile TiO_2 without other crystal phases from the XRD pattern. Rod-like morphology with a length of 160 nm and width of 50 nm and $\{10\}$ side exposed faces and $\{11\}$ and $\{01\}$ edge exposed faces were confirmed by SEM (Fig. 1a), TEM and selected area electron diffraction (SAED) analyses (data not shown). These results coincide with results of previous studies [18].

3.2. Physical and chemical properties of rutile nanorods after H_2SO_4 or H_2O_2 – NH_3 etching

XRD analysis showed that the rutile structure was retained after chemical etching, though peaks attributed to rutile became weakened and broadened, indicating that chemical etching induced surface morphological change without crystal structural changes.

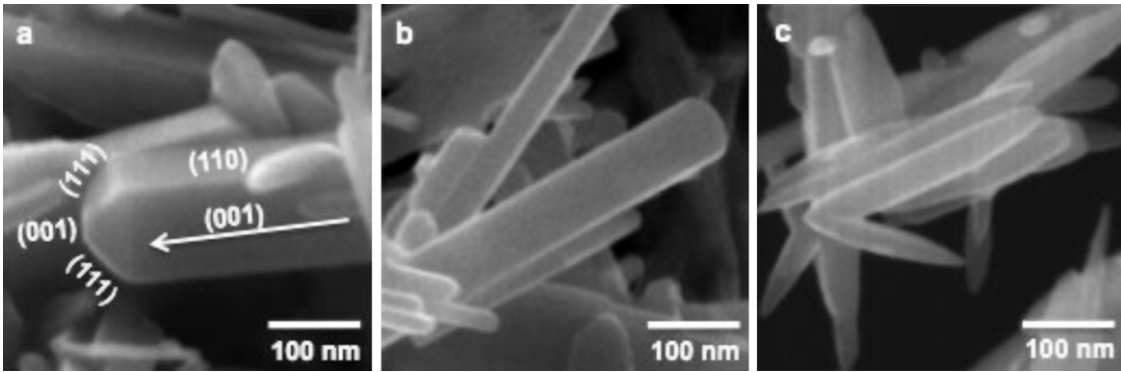


Fig. 1. SEM images of (a) nE, (b) ES and (c) EH samples.

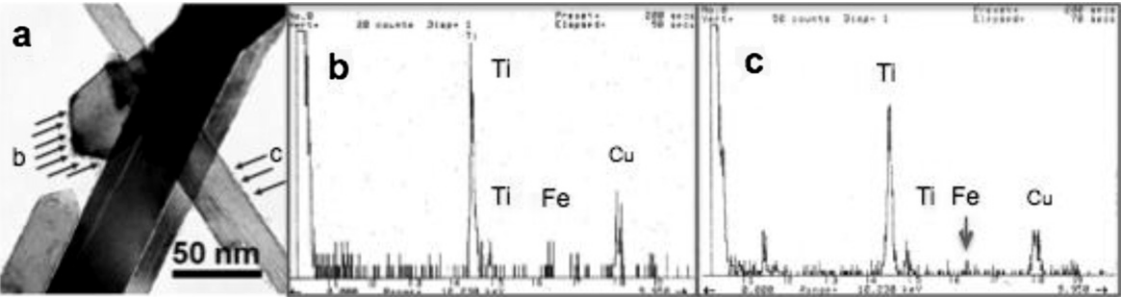


Fig. 2. TEM images (a) of nE sample with site-selective modification of Fe^{3+} ions (5 wt% of initial amount of Fe^{3+}) and EDS analysis on the edge faces (b) and the side faces (c) as indicated by arrows in (a).

In the case of H_2SO_4 etching, rutile nanorods were etched along the $[001]$ direction from the summit of the pyramid. Thus, H_2SO_4 etching for 15 h resulted in an increase in the $\{001\}$ surface area and a decrease in the $\{111\}$ surface area (Fig. 1b). On the other hand, $\text{H}_2\text{O}_2\text{--NH}_3$ etching sharpened the angle between edge faces and induced formation of a needle-like shape on the rod edge. Thus, $\text{H}_2\text{O}_2\text{--NH}_3$ etching for 1 h resulted in appearance of $\{111\}$ ($n < 1$) faces as newly exposed faces on the edge and decreased in the surface area of $\{111\}$ and $\{100\}$ faces (Fig. 1c). These results coincide with results of our previous studies [16]. Information on these synthesized samples is summarized in Table 1. In our previous study, $\{001\}$ and $\{111\}$ ($n < 1$) faces showed excellent oxidation faces for toluene decomposition under UV irradiation, compared to $\{111\}$ faces [16]. Therefore, this property is expected to induce superior site-selective modification of Fe^{3+} ions on oxidation faces.

3.3. Site-selective modification of Fe^{3+} ions on rutile nanorods after H_2SO_4 or $\text{H}_2\text{O}_2\text{--NH}_3$ etching

Site-selective modification of Fe^{3+} ions on the synthesized rutile TiO_2 was carried out. Since Fe^{3+} ions were expected to be adsorbed predominantly on oxidation reaction sites, Fe^{3+} ions were presumably modified on $\{111\}$, $\{001\}$ and/or $\{111\}$ ($n < 1$) exposed crystal faces. Site-selective modification of Fe^{3+} ions on the synthesized rutile TiO_2 was observed using TEM and energy dispersive X-ray spectroscopy (EDS). Fig. 2 shows TEM images (a) of nE sample with site-selective modification of Fe^{3+} ions (5 wt% of initial amount of Fe^{3+}) and EDS analysis on the edge faces (b) and the

side faces (c) as indicated by arrows in Fig. 2a. Fine particles were observed mainly on the edge faces (Fig. 2a), and Fe was detected by EDS analysis (Fig. 2b). In contrast, fine particles were hardly observed on the side faces (Fig. 2a), and much smaller Fe/Ti peak ratio was observed by EDS analysis (Fig. 2c). These results indicate Fe^{3+} fine particles were adsorbed mainly on the edge faces and partly on the side faces. Moreover, Fe^{3+} fine particles were observed on side faces in sample prepared without site-selective modification method (data not shown). This indicates that site-selective modification method has a large influence in adsorption of Fe^{3+} ions on oxidation faces. Table 2 shows initial and net amounts of Fe^{3+} ions modified on TiO_2 estimated by ICP-OES measurements. A larger amount of Fe^{3+} ions was modified on ES and EH samples, compared to nE samples. This indicates that an increase in S_{BET} , especially surface area of $\{001\}$ or $\{111\}$ ($n < 1$) faces, by chemical etching has an influence in an increase in adsorbed Fe^{3+} ions on TiO_2 nanorods because morphology change was mainly observed on the edge. However, Fe^{3+} adsorption depended not only on surface area of oxidation faces but also kind of exposed faces of oxidation faces. For example, a larger amount of Fe^{3+} ions was modified on ES samples than EH samples although the surface area of oxidation faces of the ES sample ($\{111\}$ and $\{001\}$ faces) was smaller than that of the EH sample ($\{001\}$ and $\{111\}$ ($n < 1$) faces). This is attributable to the adsorption property of Fe^{3+} ions depending on crystal faces. Judging from the relatively large surface area of $\{001\}$ faces of the ES sample, $\{001\}$ faces seem to be more suitable than $\{111\}$ and $\{111\}$ ($n < 1$) faces for modification of a large amount of Fe^{3+} .

Table 1
 S_{BET} and exposed crystal faces of nE, ES and EH samples.

Name	Etchant	$S_{\text{BET}}/\text{m}^2\text{g}^{-1}$	Side faces	Edge faces
nE		15	$\{111\}$	$\{111\} > \{001\}$
ES	H_2SO_4	21	$\{110\}$	$\{111\} = \{001\}$
EH	$\text{H}_2\text{O}_2\text{--NH}_3$	20	$\{110\}$	$\{111\} (n < 1) > \{111\} = \{001\}$

Table 2Initial and net amounts of Fe^{3+} ions for site-selective modification of Fe^{3+} on nE, ES and EH samples.

Sample name	Rutile rods	$\text{Fe}^{3+}(\text{init})/\text{wt}\%$	$\text{Fe}^{3+}(\text{net})/\text{wt}\%$	$\text{Fe}^{3+}(\text{net})/\text{Fe}^{3+}(\text{init})$
Fe02nE	nE	0.015	0.010	0.69
Fe05nE	nE	0.048	0.021	0.45
Fe06nE	nE	0.064	0.028	0.44
Fe03ES	ES	0.027	0.027	1.00
Fe07ES	ES	0.067	0.064	0.96
Fe13ES	ES	0.134	0.133	0.99
Fe02EH	EH	0.018	0.012	0.67
Fe06EH	EH	0.064	0.057	0.89
Fe10EH	EH	0.095	0.022	0.23

Fig. 3 shows DR spectra of bare and Fe^{3+} -modified TiO_2 . In the wavelength region between 400 and 500 nm of DR spectra, an upward shift of photoabsorption was observed. Photoabsorption was increased with an increase in the net amount of Fe^{3+} ions on ES samples. However, the relationship between photoabsorption and net amount of modified Fe^{3+} ion was not observed among ES and EH samples. This presumably indicates that Fe^{3+} ions on ES samples were site-selectively modified on $\{111\}$ and $\{001\}$ faces with high density and formed larger cluster of Fe^{3+} compound, compared to $\{111\}$ and $\{110\}$ ($\theta < 1$) faces on EH samples. Therefore, not only the amount of Fe^{3+} ions but also density of Fe^{3+} ions has an influence on photoabsorption of Fe^{3+} -modified TiO_2 .

3.4. Photocatalytic activity for toluene decomposition under visible-light irradiation

Fig. 4 shows the time course of CO_2 evolution for decomposition of toluene under visible-light irradiation. Photocatalytic activity of Fe^{3+} -modified nanorods after etching was higher than that before etching. The Fe07ES sample showed the highest activity. Its activity was 3-times higher than that of nitrogen-doped TiO_2 (N- TiO_2 ; Sumitomo Chemical Co.), which is well known as a conventional visible-light-responsive TiO_2 .

Fig. 5 shows dependence of the net amount of Fe^{3+} ions on apparent quantum yield (QY). In the case of Fe^{3+} -modified ES samples, apparent QY increased with an increase in amount of Fe^{3+} modification because of the increase in visible-light photoabsorption. On the other hand, an increase in the amount of Fe^{3+} ions decreased apparent QY in the case of Fe^{3+} -modified EH samples because an excess amount of Fe^{3+} ions decreased reduction sites by coverage of the TiO_2 surface and/or formation of inactive aggregated Fe^{3+}

species. This different behavior of photocatalytic activity despite similar amounts of Fe^{3+} ions can be explained by the adsorption property of Fe^{3+} ions on oxidation faces. Thus, a larger surface area of $\{001\}$ faces is suitable for site-selective modification of a large amount of Fe^{3+} ions. This adsorption property of Fe^{3+} ions on $\{001\}$ faces is attributed to the excellent oxidation ability of $\{001\}$ faces, where produced Fe^{2+} ions were easily recovered to Fe^{3+} ions and a larger amount of Fe^{3+} ions was modified during the modification

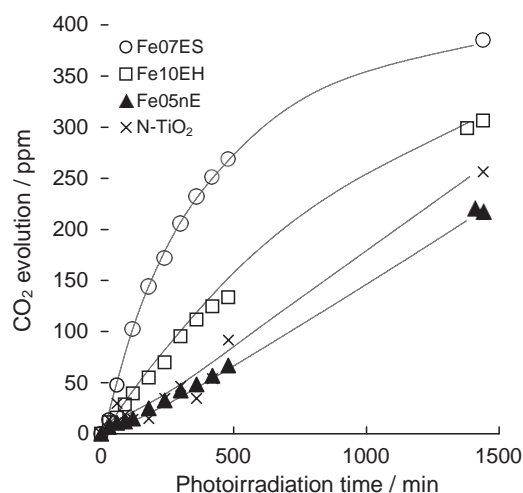


Fig. 4. Time courses of CO_2 evolution for toluene decomposition over N-doped TiO_2 (\times) and ES sample (\circ) EH sample (\square) and nE sample (\blacktriangle) with site-selective modification of optimum amount of Fe^{3+} ions.

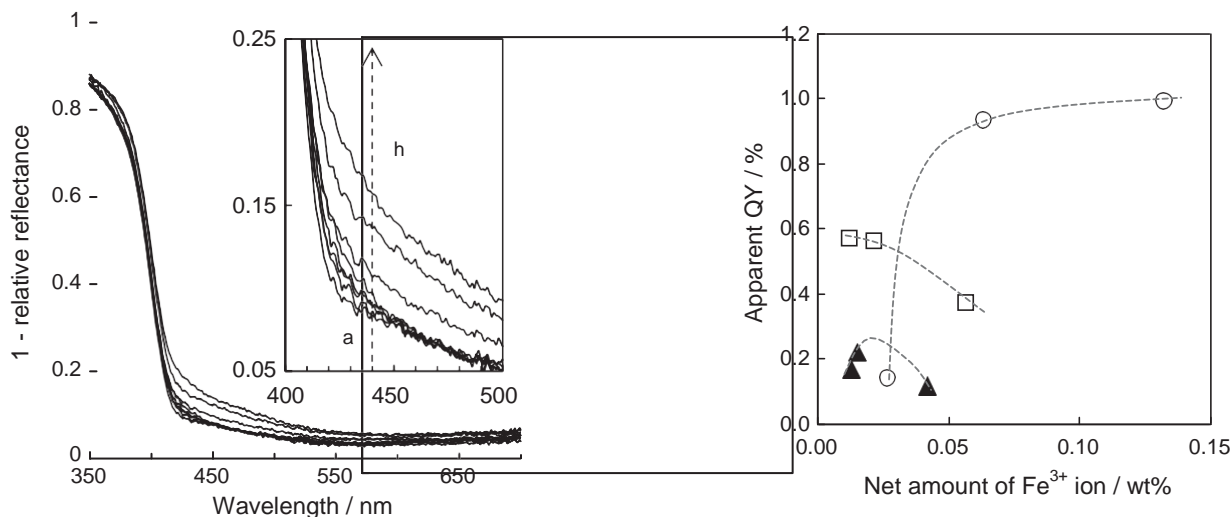


Fig. 3. DR spectra of (a) bare and Fe^{3+} -modified TiO_2 (b) Fe03ES, (c) Fe05nE, (d) Fe07ES, (e) Fe13ES, (f) Fe06EH, (g) Fe02EH and (h) Fe10EH.

Fig. 5. Relation between net amount of Fe^{3+} ions and apparent quantum yield for photocatalytic toluene decomposition. ES samples (\circ), EH samples (\square) and nE samples (\blacktriangle) with site-selective modification of Fe^{3+} ions.

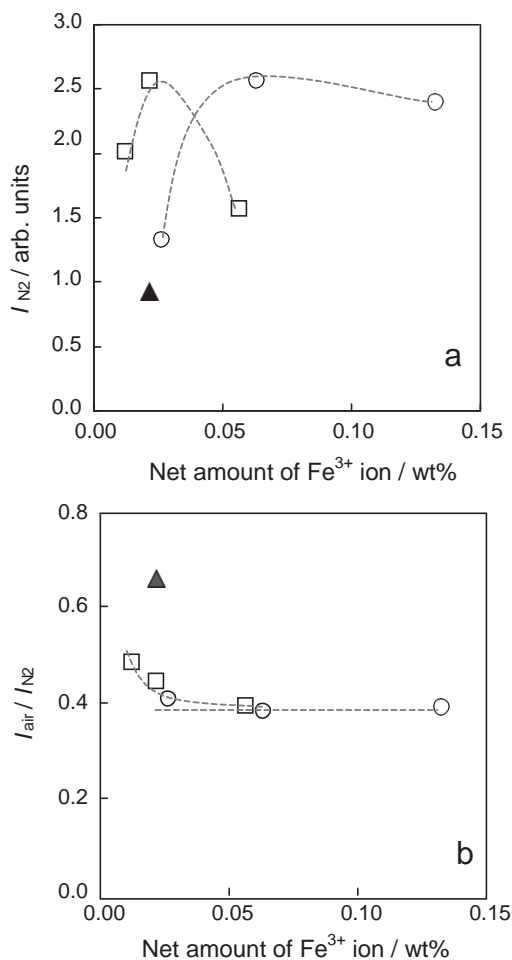


Fig. 6. Relation between net amount of Fe³⁺ ions and (a) I_{N_2} , and (b) ratio of I_{air} to I_{N_2} . ES samples (○), EH samples (□) and nE samples (▲) with site-selective modification of Fe³⁺ ions.

procedure, compared to other exposed faces ($\{1\ 1\ 0\}$ and $\{1\ 1\ n\}$ ($n < 1$) faces).

Fe³⁺-modified EH samples showed higher activity than that of Fe³⁺-modified nE samples due to the larger surface area of oxidation faces $\{1\ 1\ n\}$ ($n < 1$), resulting in modification of highly dispersed

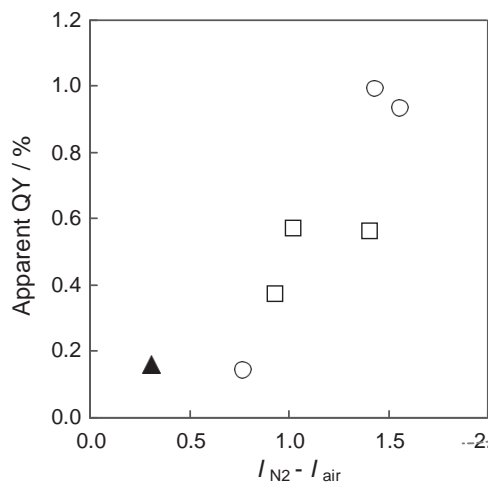


Fig. 7. Relation between $I_{N_2} - I_{air}$ and apparent quantum yield for photocatalytic toluene decomposition. ES samples (○), EH samples (□) and nE samples (▲) with site-selective modification of Fe³⁺ ions.

Fe³⁺ ions on oxidation sites. However, the activity of Fe³⁺-modified EH samples was not as high as that of Fe³⁺-modified ES samples, because $\{1\ 1\ n\}$ ($n < 1$) faces have an inferior adsorption property of Fe³⁺ ions, resulting in a smaller amount of site-selective Fe³⁺ modification, compared to $\{0\ 0\ 1\}$ faces.

In order to discuss adsorption stability of Fe³⁺ ions on TiO₂ surfaces, the powders after photocatalytic reaction were rinsed with deionized water and the rinsing water was filtered and analyzed by ICP-OES. However, Fe³⁺ ions in the rinsing water were hardly detected by ICP-OES. Moreover, DR spectrum of post-reaction sample after the rinsing was almost same as that of pre-reaction one (data not shown). From these results, it was demonstrated that the adsorption of Fe³⁺ ions is stable in gaseous condition under photoirradiation.

3.5. DB-PA spectroscopic detection of electron behavior under visible-light irradiation

The behavior of electrons injected into rutile TiO₂ was observed by DB-PAS [19]. At first, time-course curves of PA intensity for Fe³⁺-modified rutile nanorods in the presence of N₂ + EtOH were obtained. PA intensity increased with visible-light irradiation because Ti⁴⁺ was reduced to Ti³⁺ by injected electrons from photoexcited Fe³⁺ ions [15]. Thus, increase in PA intensity is attributed to the amount of injected electrons in TiO₂. Fig. 6a shows the relation between net amount of Fe³⁺ ions and saturation limit of PA intensity under N₂ + EtOH (I_{N_2}). The I_{N_2} of Fe³⁺-modified nanorods after etching was larger than that before etching. This indicates that enhancement of photocatalytic activity by morphological change of oxidation faces was due to an increase in the amount of injected electrons. Thus, newly exposed $\{0\ 0\ 1\}$ and $\{1\ 1\ n\}$ ($n < 1$) faces were suitable faces for modification of Fe³⁺ ions, which inject a large amount of electrons into TiO₂.

Time-course curves of PA intensity for Fe³⁺-modified rutile in the presence of air + EtOH were also obtained. PA intensity attributed to Ti³⁺ formation was greatly decreased because electron accumulation was retarded due to electron consumption by oxygen species on the TiO₂ surface. Therefore, efficiency of reduction by injected electrons can be estimated using the saturation limit of PA intensity under air + EtOH (I_{air}). Fig. 6b shows the relation between net amount of Fe³⁺ ions and ratio of I_{air} to I_{N_2} . Fe³⁺-modified EH samples showed a larger ratio of I_{air} to I_{N_2} than did Fe³⁺-modified ES samples. This is because formation of $\{1\ 1\ n\}$ ($n < 1$) faces decreases the surface area of $\{1\ 1\ 0\}$ faces, which work as reduction reaction faces.

Fig. 7 shows apparent QY as a function of difference between $I_{N_2} - I_{air}$, which expresses the amount of electrons that were injected from Fe³⁺ ions into TiO₂ and reacted with O₂ on the TiO₂ surface. These values show a positive correlation among all of the prepared samples. Thus, high activity of Fe³⁺-modified ES samples was attributed to both large $\{0\ 0\ 1\}$ faces as focused Fe³⁺ adsorption sites and maintenance of $\{1\ 1\ 0\}$ faces as reduction sites.

4. Conclusion

We demonstrated that Fe³⁺ ions were modified on newly exposed crystal faces of rutile nanorods, which were formed by chemical etching. Fe³⁺-modified rutile nanorods after chemical etching showed higher photocatalytic activities for degradation of toluene under visible-light irradiation. This is because newly exposed crystal faces ($\{0\ 0\ 1\}$ and $\{1\ 1\ n\}$ ($n < 1$) faces) were suitable faces for modification of Fe³⁺ ions, which inject a large amount of electrons into TiO₂. Optimized Fe³⁺-modified ES samples showed excellent photocatalytic activity because a large amount of Fe³⁺ ions was site-selectively modified on oxidation faces due to high

oxidation ability of {001} faces. On the other hand, photocatalytic activity of Fe³⁺-modified EH samples was not as high as that of optimized Fe³⁺-modified ES samples. DB-PAS measurements indicated that the reason for this was slow consumption of injected electrons as a result of decrease in surface area of {110} faces as reduction faces and less site-selectivity of Fe³⁺ modification.

Acknowledgements

This work was supported by the Knowledge Cluster Initiative implemented by the Ministry of Education, Culture, Sports, Science and Technology (MEXT), the JST PRESTO program, and the JST ACT-C program.

References

- [1] W. Choi, A. Termin, M.R. Hoffmann, *Journal of Physical Chemistry* 98 (1994) 13669–13679.
- [2] N. Serpone, D. Lawless, *Langmuir* 10 (1994) 643–652.
- [3] H. Kisch, L. Zang, C. Lange, W.F. Maier, C. Antonius, D. Meissner, *Angewandte Chemie International Edition* 37 (1998) 3034–3036.
- [4] S. Sato, *Chemical Physics Letters* 123 (1986) 126–128.
- [5] R. Asahi, T. Morikawa, T. Ohwaki, K. Aoki, Y. Taga, *Science* 293 (2001) 269–271.
- [6] T. Umebayashi, T. Yamaki, H. Itoh, K. Asai, *Applied Physics Letters* 81 (2002) 454–456.
- [7] T. Ohno, M. Akiyoshi, T. Umebayashi, K. Asai, T. Mitsui, M. Matsumura, *Applied Catalysis A: General* 265 (2004) 115–121.
- [8] T. Ohno, T. Tsubota, K. Nishijima, Z. Miyamoto, *Chemistry Letters* 33 (2004) 750–751.
- [9] H. Irie, Y. Watanabe, K. Hashimoto, *Chemistry Letters* 32 (2003) 772–773.
- [10] L. Zang, C. Lange, I. Abraham, S. Storck, W.F. Maier, H. Kisch, *Journal of Physical Chemistry B* 102 (1998) 10765–10771.
- [11] L. Zang, W. Macyk, C. Lange, W.F. Maier, C. Antonius, D. Meissner, H. Kisch, *Chemistry: A European Journal* 6 (2000) 379–384.
- [12] S. Ikeda, N. Sugiyama, B. Pal, G. Marci, L. Palmisano, H. Noguchi, K. Uosaki, B. Ohtani, *Physical Chemistry Chemical Physics* 3 (2001) 267–273.
- [13] W. Macyk, H. Kisch, *Chemistry: A European Journal* 7 (2001) 1862–1867.
- [14] T. Ohno, D. Haga, K. Fujihara, K. Kaizaki, M. Matsumura, *Journal of Physical Chemistry B* 101 (1997) 6415–6419.
- [15] N. Murakami, A. Ono, M. Nakamura, T. Tsubota, T. Ohno, *Applied Catalysis B: Environmental* 97 (2010) 115–119.
- [16] E. Bae, N. Murakami, M. Nakamura, T. Ohno, *Applied Catalysis A: General* 380 (2010) 48–54.
- [17] E. Hosono, S. Fujihara, K. Kakiuchi, K. Imai, *Journal of the American Chemical Society* 126 (2004) 7790–7791.
- [18] E. Bae, N. Murakami, T. Ohno, *Journal of Molecular Catalysis A: Chemical* 300 (2009) 72–79.
- [19] N. Murakami, O.O.P. Mahaney, R. Abe, T. Torimoto, B. Ohtani, *Journal of Physical Chemistry C* 111 (2007) 11927–11935.